AIAA SciTech Forum
7-11 January 2019, San Diego, California
AIAA Scitech 2019 Forum

10.2514/6.2019-2023

Detonation Structure in Ethylene/Air based Non-premixed Rotating Detonation Engine

Takuma Sato* and Venkat Raman†
The University of Michigan, Ann Arbor, MI 48109-2102, USA

Rotating Detonation Engines (RDEs) are getting more attention as a new pressure gain combustion system. In order to use RDEs to augment practical gas turbines, their stability and performance with more applicable hydrocarbon fuels need to be tested. In this context, ethylene/air systems are useful in analyzing RDE performance. Prior work has shown that ethylene/air systems exhibit suppressed wave propagation, with speeds that are nearly half the ideal wave speeds. The purpose of this study is to simulate realistic RDE configurations that have been experimentally studied to gain insight into this wave suppression. Detailed numerical simulations using a 21-species 38-steps chemistry model and a reduced 8-species 2-step model are conducted. When ethylene is diluted with hydrogen, the system exhibits two different wave modes, with a strong mode that is comparable to detonation propagation and a weak mode that behaves more like a deflagaration process. It is further shown that pure ethylene cases stay in the weak regime and contain only a weak pressure propagation that is aided by deflagaration along the wave path. As a result, the observed wave is not based on a conventional detonation structure.

I. Introduction

Pressure gain combustion has been gaining attention over the last decade, primarily due to its ability to extend gas turbine performance by providing significant efficiency gains [1–4]. More recently, rotating detonation engines (RDEs) have become the design choice for achieving pressure gain in a practical system. Figure 5 shows a simulation of a canonical RDE geometry designed by Air Force Research Laboratory (AFRL) as well as the main flow features. In such RDEs, a detonation wave moves azimuthally in an annular chamber, processing fuel/air mixtures that are fed through ports at the base of the chamber. Since detonations typically propagate at very high speeds, the effective thrust producted by the system is nearly continuous, albeit with an azimuthal component. This is the main difference from the conventional pulse detonation engines (PDEs), where the detonations are spaced in time due to the requirement of filling the detonation chamber every cycle [4]. As seen in Fig. 6, the detonation wave exhibits a complex structure, where inhomogeneous fuel-air mixture is processed by the shock-wave that propagates in the chamber. The compression generated by the shock-wave provides the pressure gain that can be converted into useful work. For this efficiency to be realized, there should be minimal pressure losses inside the combustor. More importantly, a sustained detonation front needs to exist. The main design challenge is in configuring the fuel and air inflow streams. As the detonation wave passes over these injectors, it can cause reverse flow that pushes product and partially-burnt gases into the feed plenums. This effect will lead to premature reactions, causing a reduction in detonation efficiency. One way to stop this reverse flow is by using a high feed pressure, which in itself will lead to cycle losses. Hence, the objective of the feed plenum design is to minimize the stiffness of the injectors (i.e., the feed pressures required) while reducing the impact of the reverse flow.

Another aspect of RDE design is the impact of fuel on the detonation and fuel/air mixing processes. While much of the early work has been on hydrogen/air systems [5, 6], a variety of other fuels have also been considered. In general, hydrocarbon fuels are harder to detonate in comparison to hydrogen, which implies that special design considerations are needed. An important metric for detonability is the cell size, determined based on soot foil experiments [7]. In general, the width of the detonation chamber as well as the height to which the fuel-air mixture is filled before a detonation wave is encountered are both sensitive to this detonation cell size [8, 9]. In general, this is related to the propagation of triple points, which are regions of high pressure formed by interacting shocks that provide fast ignition. Hence, fuel mixtures that detonate slower require larger channels in order to accommodate the formation and propagation of these triple point structures.

*PhD Student, Department of Aerospace Engineering, takusato@umich.edu
†Professor, Department of Aerospace Engineering, AIAA Associate Fellow, ramanv@umich.edu

Due to increasing interest in the use of RDEs for nearly all gas turbine applications, there has been studies using methane [10, 11], ethylene [12–14], propane [15, 16] and more practical fuels such as JP-10 [17]. In these studies, some focus on extensive flow field computations [2, 18], while others are focused on the detonation characteristics [16, 17]. While there are substantial differences in the detonation characteristics of these fuels, many of these studies are conducted at conditions where strong detonations are present in the system. Invariably, the detonation waves propagate at conditions close the CJ speed. In fact, in most studies that consider uniform mixtures, the propagation speed is very close to this theoretical value [19]. However, it has been noted that when discrete injection is present, the wave speed can be significantly altered [14, 20–22]. For instance, Fujii et al. [14] showed that the detonation velocity can go down to 86% of the CJ speed for ethylene/oxygen based discrete injection. However, the aforementioned studies were performed in linearized systems where a single wave passes through the set of injectors. Full-scale RDEs have been used to study hydrocarbon mixtures [10, 12, 13]. Of these, the ethylene/air systems studied by Wilhite et al. [13] and Cho et al. [12] show some interesting features. Both consider ethylene/air injection albeit with slightly different injection schemes. However, in both studies, the detonation wave velocity is much smaller than CJ speed, and operating only slightly below the sound speed of post-detonation conditions (roughly 1000 m/s). This is nearly 50% of the ideal CJ wave speed. In both studies, this low detonation speed was observed over a range of operating conditions. One explanation is that the fuel-air mixing is not sufficiently complete to ensure a fast propagating detonation wave. It has been hypothesized that a reduction in wave velocity is related to inefficient fuel-air mixing. However, other effects could also be present. For instance, Sato et al. [23] showed that during the fuel/air refill, there could be ignition due to contact with the burnt gases from the previous cycle. As a result, the detonation wave encounters a partially-burnt and inhomogeneous mixture, which can dramaticlly reduce detonation efficiency. For instance, in one of the case studies [23], it was shown that the pre-burning can reduce peak pressure by nearly 40%, thereby affecting the wave propagation speeds. Hence, practical systems can generate a complex flow structure that can limit the detonation speed.

Given this background, the focus of this work is to obtain insight into the flow features of an ethylene/air based RDE. The simulation configuration is based on the experiment of Cho et al. [12]. In particular, of interest is the detonation wave structure that supports a weak propagation. For this purpose, detailed numerical simulations are conducted. One aspect that requires some discussion is the description of flame kinetics. In most detonation calculations, one step chemistry or reduced order models such as the induction parameter model [11, 24] are used. If the detonations are strong enough such that the propagation speed is close to CJ speed, then such methods have been shown to be reliable in a number of studies. While detailed kinetics models are widely used in combustion simulations, these models have been developed predominantly for deflagrations, and their direct application to detonation calculations still need to be evaluated. To address these issues, the simulations conducted here use both detailed chemical kinetics as well as a detonation-specific reduced order model for ethylene. Several canonical flows are tested to determine the suitability of this approach.

II. Computational Approach

The numerical simulations solve the full set of governing equations for compressible fluid flow given below.

$$\frac{\partial \rho}{\partial t} + \frac{\partial \rho u_i}{\partial x_i} = 0, \tag{1}$$

$$\frac{\partial \rho u_i}{\partial t} + \frac{\partial \rho u_i u_j}{\partial x_j} = -\frac{\partial p}{\partial x_i} + \frac{\partial \tau_{ij}}{\partial x_j}, \tag{2}$$

$$\frac{\partial \rho E}{\partial t} + \frac{\partial \rho u_j H}{\partial x_j} = \frac{\partial}{\partial x_j} k \frac{\partial T}{\partial x_j} + \frac{\partial \tau_{ij} u_i}{\partial x_j}, \tag{3}$$

$$\frac{\partial \rho Y_i}{\partial t} + \frac{\partial \rho u_j Y_i}{\partial x_j} = \frac{\partial}{\partial x_j} \rho D \frac{\partial Y_i}{\partial x_j} + \dot{\omega} M_i, \tag{4}$$

where ρ is the mass density, u, v, w are x, y, and z velocity components, respectively, p is the pressure, E is the total energy, and H is the total enthalpy. For each species $i = 1, \ldots, N$, where N is the number of species, Y_i is the mass fraction, $\dot{\omega}_i$ is the molar production rate, and M_i is the molecular mass. For the simulations discussed here, the viscous and diffusive terms are neglected, and the equations are solved in the Euler limit. Although this changes the near-wall behavior and heat transfer, the mixing and detonation processes are still dominated by the inertial terms. Several prior

studies have confirmed (for instance, [25]) that the use of the full Navier-Stokes equations did not appreciably change the results, especially when heat transfer was not critical.

The full-scale RDE consists of a complex geometric design that requires the computational solver to account for a multitude of fuel and air injectors. As a result, the computational tool should be able to handle this complex geometry and the underlying flow physics. To this end, the OpenFOAM open source code base is used as the starting point. This software framework is capable of handling complex flow geometries. In order to accurately solve detonation physics, the UM research group has developed an in-house package based on OpenFOAM, UMdetFoam. UMdetFOAM combines highly accurate spatial and temporal discretization of governing equations with CANTERA-based [26] determiniation of chemical source terms. The solver and its low-Mach number version have been validated on a number of flows [19, 23, 27–33]. MUSCL-based HLLC and second-stage Runge-Kutta are utilized for spatial and time discretization, respectively. Diffusion terms are discretized by Kurganov, Noelle and Petrova (KNP) method [34]. By coupling CANTERA along with Finite Volume Methods (FVM) of the OpenFOAM platform, arbitrary detailed kinetics can be simulated.

In this study, the Varatharajan mechanism (38 steps with 21 species) for ethylene [35] was utilized as the detailed mechanism. This model has been previously tested for detonation problems. In particular, Sato et al. [25] used this mechanism to study ethylene/air detonations in a two-dimensional unwrapped configurations using the UMdetFOAM solver. Considerable validation efforts were described in that work and are not repeated here. In order to increase the computational speed, a reduced-order two-step mechanism of Varatharajan et al. [17] is used. The ethylene/air mechanism transports eight species with only two steps. The source terms $\dot{\omega}_i$ can be analytically computed to reduce the computational time. However, to ensure that the choice of chemistry mechanisms does not unduly affect the conclusions, several canonical flows are tested first.

III. Computational results

The first two sections below describe the verification/validation effort in order to determine to ensure that the two-step reduced mechanism is suitable for the conditions used in this work. Further, these simplified test cases provide a basis of comparison with the more detailed calculations presented in Sec. III.D.

A. One-dimensional detonation case

To validate the two-step mechanism, a one-dimensional detonation tube calculation is first performed. Here, a uniform mixture of stoichiometric ethylene/air is filled at initial time. The domain is of length $L = 0.3$ m, filled with ethylene/ air mixture at stoichiometric condition, with a pressure of 1 atm and temperature of 300 K. The left boundary is treated as a wall while the right boundary is open with zero gradient conditions (purely convective flow). At initial time, a high energy region is patched closed to the wall. In the simulation, this leads to the profile shown in Fig. 1. This particular calculation used a grid size of $dx = 5 \times 10^{-5}$m. The 1D profile shows a sharp peak corresponding to the von Neumann pressure, which reaches a value of nearly 30 atm for this fuel mixture. The temperature profile shows a similar rise due to the shock and a slow expansion that reduces the temperature until ignition provides a net energy release.

Figure 2 shows the detailed species behavior and the pressure profile across the detonation front. It is seen that the fuel and oxidizer are consumed as the pressure significantly increases. When the pressure reaches its peak value along with the intermediate species, the consumption of the reactant mixture and the production of the product gases are completed.

To study grid dependence, the error in peak pressure and wave speed relative to the finest resolution ($dx = 3 \times 10^{-5}$m) is plotted in Fig. 3. It can be seen that the peak pressure monotonically converges with grid resolution. Wave speed, which has a more complex dependence on grid resolution due to the impact of species evolution, shows a non-monotonic convergence. This aspect is well-known in detonation simulations [36]. It is also important to recognize that the error in wave speed is less than 1% even at the coarsest resolution. Overall, a resolution of $100 - 400\mu$m is deemed sufficient for ensuring good grid quality.

B. Two-dimensional detonation case

Two dimensional detonations occurring in confined channels have been used to understand the shock wave structure [19, 23, 36, 37]. In particular, when a channel filled with fuel-air mixture is ignited, it transitions to detonating flow and forms characteristic cellular patterns that can be observed by recording shock impact on the side-walls using a soot-coated foil. This flow configuration is simulated here using the two-step chemistry mechanism. Here, the

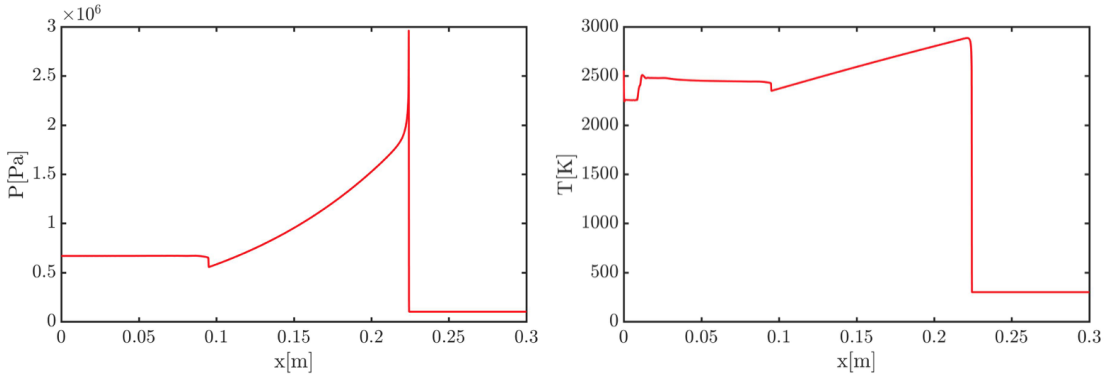

Fig. 1 Pressure and temperature profiles in 1D detonation tube.

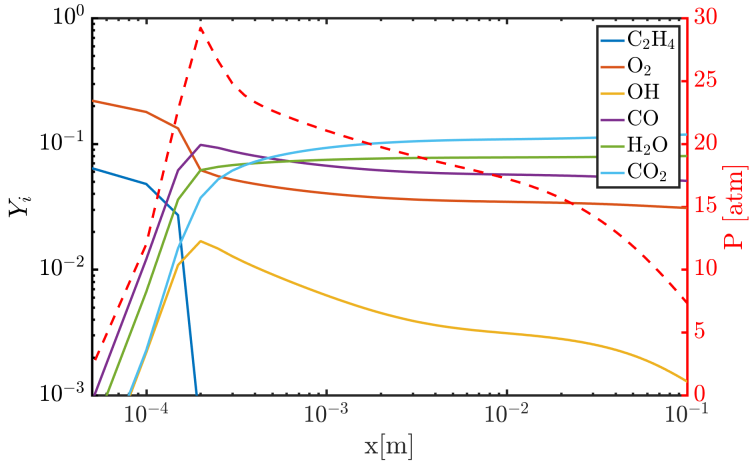

Fig. 2 Detailed species behavior across the detonation wave, where the x axis represents the distance behind the wave front.

computational domain consists of a channel of height $h = 2 \times 10^{-3}$ m and length $L = 3 \times 10^{-2}$ m. The grid size is set to $dx = 2.5 \times 10^{-6}$ m. This two-dimensional channel is filled with ethylene/ air mixture at stoichiometric condition, with a pressure of 0.1 atm and temperature of 300 K. This condition has been previously studied by Araki et al. [36]. The cellular structure is visualized by tracking the local maximum pressure at the shock front as a function of time. Figure 4 shows the cellular structure with the two-step mechanism (bottom) and the detailed mechanism (top). Compared to the detailed mechanism, the two-step mechanism forms a smaller cell structure. However, prior studies with reduced-order detonation models [11] provide similar cell sizes as observed here. It is known that chemical mechanisms have a significant impact on cellular structure [38]. For the analysis below, it is important to consider these variations. For these reasons, the detailed and reduced mechanisms are used wherever feasible.

C. Simulation configuration

The RDE configuration simulated here is based on the AFRL design used in [12]. This design is similar to the hydrogen/air RDEs used in other related studies [6], but has a larger annulus width to account for the slower ethylene/air chemistry and to sustain the triple points/cell size.. Due to this change, the fuel-air mixing is different compared to the hydrogen-based RDE. Figure 5 shows the overview of this geometry. The channel width is 22.86 mm, and the area ratio between the oxidizer inlet and the detonation chamber is 0.059 [12]. The air injection slot is 1.778 mm wide. The oxidizer stream and the fuel stream vertically intersect at the bottom of the chamber.

Several different simulations are conducted here, but one of the main variations is in the dilution of the fuel with

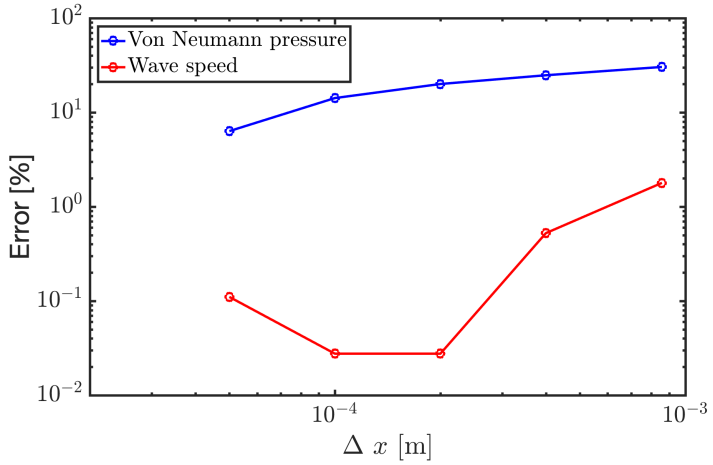

Fig. 3 Convergence of von Neumann pressure and wave speed with grid sizing in 1D detonation tube cases with C_2H_4/Air with 300K, 1 atm.

hydrogen gas to study its impact. A list of simulations studies here are provided in Table. 1. The air mass flow rate is set to 0.7 kg/s for the pure ethylene fuel cases. The total temperature in the air plenum is varied between 400 K, 600 K, and 800 K. T_0 = 300 K is used for the fuel plenum in every case. The back pressure is 1 atm and 2 atm for the pure ethylene and ethylene with hydrogen addition cases, respectively. The increase in back pressure for the ethylene with hydrogen addition case increases the baseline pressure in the detonation chamber, thereby increasing the detonability of the mixture. The total pressure in the each plenum is computed by the choke relation as follows,

$$P_0 = \frac{\dot{m}}{A}\left(1 + \frac{1}{2}(\gamma - 1)\right)^{\frac{\gamma+1}{2(\gamma-1)}}\sqrt{\frac{RT_0}{\gamma}} \tag{5}$$

where A is the area, R is the gas constant of each stream, γ is the specific heat ratio, and $\dot{m}$ is the target mass flow rate. When oxidizer plenum total temperature is changed, it affects the post-throat pressure in the detonation chamber, impacting both the detonation as well as the fuel-air mixing process by altering the injection velocities for the same mass flow rate. These variations will help understand the role of mixing effects on the wave speed.

Composition	Oxidizer plenum P_0 (kPa)	Fuel plenum P_0 (kPa)	Oxidizer plenum T_0 (K)	Fuel plenum T_0 (K)	Air mass flow rate (kg/s)	Back pressure (atm)	Computed wave velocity (m/s)
C_2H_4/Air	509	292	400	300	0.7	1	766
C_2H_4/Air	623	292	600	300	0.7	1	978
C_2H_4/Air	720	292	800	300	0.7	1	1153
C_2H_4:H_2(50:50)/Air	441	420	300	300	0.7	2	993

Table 1 Test case description as well as summary of macroscopic results from the simulations.

A baseline computational grid is generated with the minimum grid spacing of 3 $\times 10^{-4}$ m and 1.5 $\times 10^{-4}$ m for the pure ethylene and ethylene with addition of hydrogen, respectively. The smaller mesh size for the hydrogen addition case is to accommodate the faster chemistry expected in this case. The mesh near the injection system is shown in Fig. 5. The total number of computational volumes range from 15 to 80 million cells depending on the mesh resolution. Prior studies [5, 23] of similar AFRL configurations show that such refined mesh is necessary to capture the detonation processes.

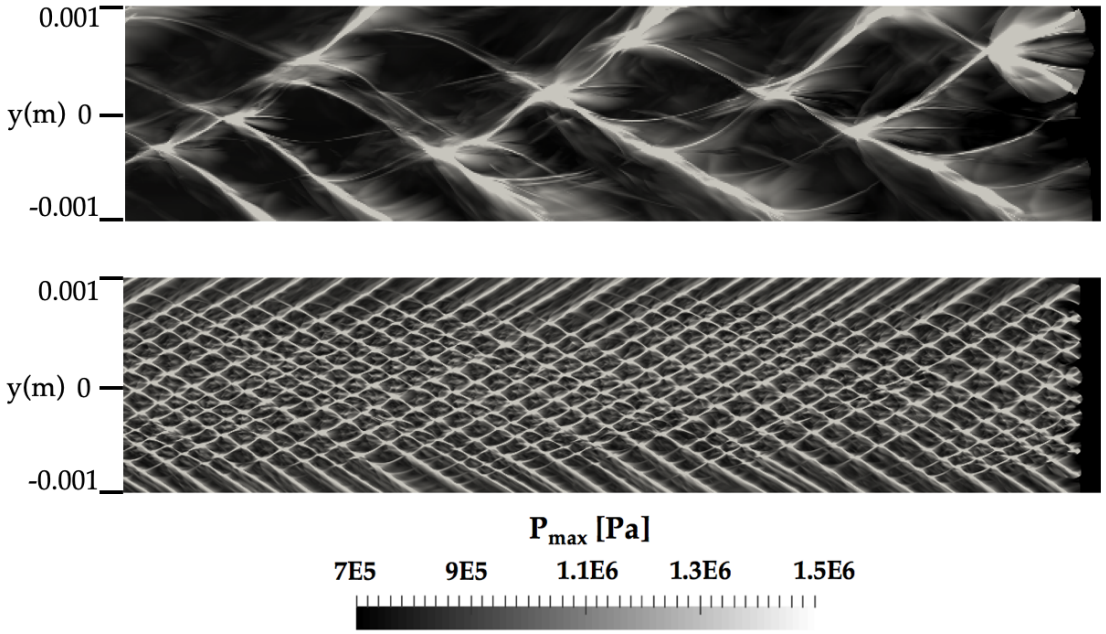

Fig. 4 Detonation cell structure derived from the maximum pressure history for the detailed chemical mechanism (top) and the two-step mechanism (bottom).

The simulations are performed as follows. Starting with a uniform flow field, the fuel and oxidizer jets are allowed to evolve in the domain without any chemical reactions. Once this development is complete and fully-choked conditions are established for both sets of injectors, a high temperature region is patched within the annulus with gas conditions replicating the one-dimensional post-detonation values (obtained from 1D simulation data). This flow is allowed to evolve for sufficient time until a statistically stationary detonation field is observed. Note that the time required to reach this state is highly dependent on the flow and initial conditions. After reaching this stationary state, the simulation is continued and data is collected for evaluating statistics such as wave velocity or shock structure. The total simulation time for this phase is equivalent to roughly 4-5 cycle periods after reaching steady state. In the discussions below, only results from this phase will be presented.

D. Ethylene/hydrogen case

The case of ethylene fuel with hydrogen addition is discussed first since a) it is computed using the detailed chemical mechanism which has been extensively validated before, and b) it serves as a baseline for the discussion about the pure ethylene cases.

The first important metric to note is the wave velocity, which is provided in Table. 1. Consistent with the experiments, the wave velocity is less than 1000 m/s, even though the CJ velocity for this mixture is computed at 1830 m/s. A closer look at the simulation data shows that even after reaching a quasi-steady state, the combustor exhibits two wave modes, which are termed strong and weak modes here. Figure 6 shows the pressure profiles for these two modes. As observed, the peak pressure reaches roughly 12 atm in the strong mode and nearly half that value in the weak mode. Over the 5 cycle time this simulation was run, the wave modes switched many times. In the strong mode, the wave structure is reminiscent of the hydrogen-based RDE [5, 23]. However, the oblique shock formed above the primary detonation wave is weaker with a shallower angle. This indicates that the wave itself is moving slower than CJ speeds. This detonation structure is also different from the two-dimensional unwrapped RDE simulations [11, 25], where ethylene-based combustors did not show a significant difference in wave structure compared to hydrogen-based combustors. Hence, the strong mode itself is weaker than a CJ-speed-based wave structure.

The weak mode seems to have a more complex structure with a region of relatively low pressure rise with higher curvature and thickness in comparison to the strong mode. This structure is similar to the weakened shock structure observed in linear RDEs [21, 39], caused by the detachment of the reaction zone from the leading shock wave. Over

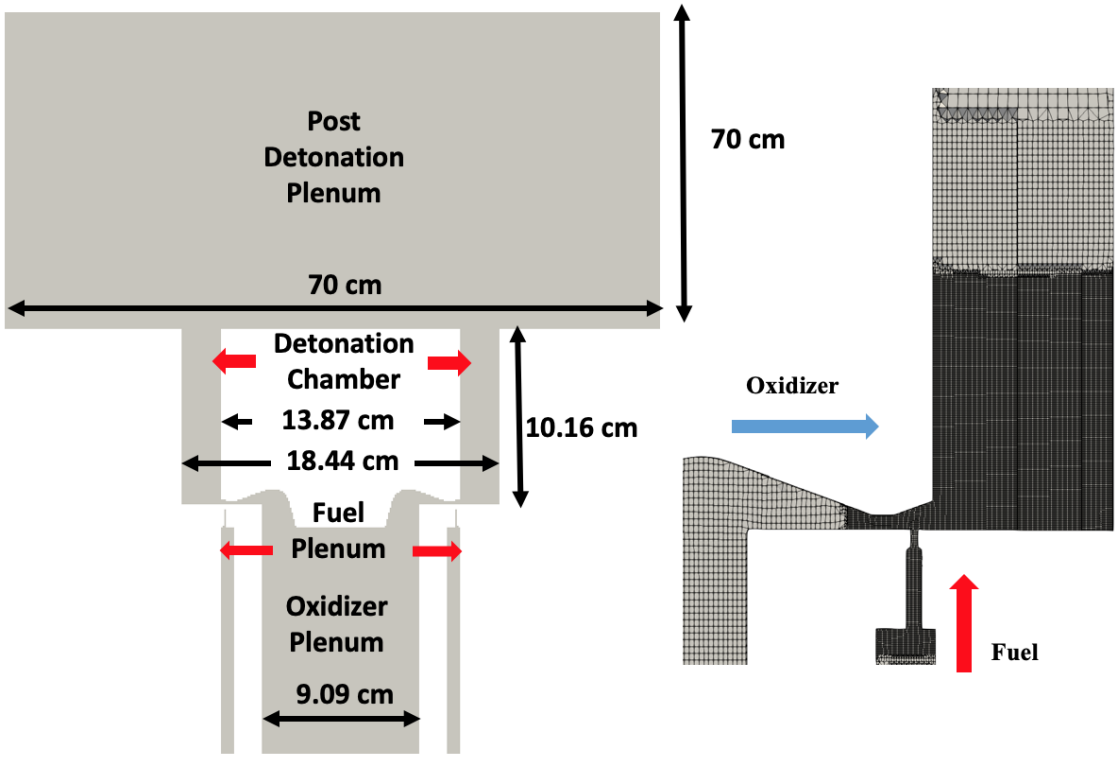

Fig. 5 Left: Computational geometry and RDE configuration with dimensions. Right: the fuel and oxidizer injection scheme with computation mesh.

many cycles, the weak wave interacts with other reflected waves within the domain and can coalesce to form a strong mode.

It is important to note that these pressure waves are not uniform across the channel width. To illustrate this feature, the middle row in Fig. 6 shows the pressure field in the center of the channel at same time instant as the pressure at the outer wall on the top row. It is seen that for both the strong and weak modes, the pressure profile in the middle of the channel is much weaker than the outer diameter pressure values. These differences indicate that there are considerable variations in the local conditions across the chamber.

This feature is more visible in the bottom row in Fig. 6, which shows a plane perpendicular to the axis of the RDE. It is seen that the pressure wave is uniform across the chamber in the strong mode but is very weak and irregular in the weak mode. In fact, there is no clear wave front visible in the weak mode.

These variations are reflected in the temperature profiles as well. Figure 7 shows the temperature profile for the two modes. It is seen that in the strong mode, there is clear separation between the low temperature refill region ahead of the wave, and the post-detonation hot gases. However, the weak mode only contains sporadic ignition regions or hotspots. The mid-channel profiles (the middle row in Fig. 7) show a highly reactive but non-wave-like structure for the weak mode and a detonation-like structure for strong mode. In the cross-sectional view, it can be seen that the strong mode has the characteristics of a detonation wave, while the weak mode behaves similar to a homogeneous ignition reactor. As a result, there are no clear wave fronts but regions of high temperature that are slowly being convected out of the domain.

To understand the causal mechanisms, the local equivalence ratio in the domain is plotted. The top row in Fig. 8 shows the profile near the outer wall while the middle row in Fig. 8 shows the profile at half the channel width. Although the global equivalence ratio is 1 for these studies, the local equivalence ratio varies substantially, from 0 to 2 across most of the domain. While the strong mode shows a leaner mixture at the mid-channel and outer wall locations (roughly stoichiometric), the weak mode contains values close to stoichiometric at the middle of the channel and richer mixtures near the walls. The top view (the bottom row in Fig. 8) shows a similar structure with larger variations in the weak mode in comparison to the strong mode.

From this data, it can be concluded that the system exhibits multiple modes of operation. As the detonation wave

passes an injector, it causes the fuel and oxidizer injection to become unchoked. At that stage, the time it takes for the injectors to recover is dependent upon the plenum pressure and the specific design. From prior studies [23], it is known that the fuel and oxidizer injectors recover at different rates. This causes the local equivalence ratio to be vastly different from the nominal value of 1. If the mixing is not rapid enough to homogenize this mixture, the detonation wave arrives too soon, causing a weakening of the wave. However, due to the complex wave structure inside the domain, the injectors return to a synchronized mode over several cycles, at which point a coherent strong wave mode is formed.

However, even the strength of the strong mode is dependent on the level of homogenization. It is clear that once the mixing is sufficiently efficient, the waves re-stabilize at the strong mode. However, the presence of the wave itself causes the injectors to be thrown out of synchronization. Hence, two different time scales can be defined. The larger time scale is the time to synchronization that depends on the chamber dynamics and the injector mixing process. The smaller time scale is related to the level of homogenization possible before a strong wave is established. The effective velocity is then some linear combination of these two wave modes, with the effect of each mode dependent on the large time scale, while the strength of each mode is dependent on the shorter time scale.

The original intent of adding hydrogen was to determine whether the combustor will be able to operate in a purely detonating mode. It is clear that even with 50% addition, the hydrocarbon ignition controls the process. It is expected that as hydrogen fraction increases, the combustor will spend longer durations in the strong wave mode, with the strength this mode increasing due to the wider detonability range (as a function of equivalence ratio) of hydrogen.

E. Pure ethylene cases

Given the structure of the detonation wave observed in the ethylene/hydrogen blend, the next set of cases analyze the pure ethylene cases and the structure of combustion for several operating conditions. To begin with, Table. 1 that the wave velocity is again very low compared to ideal CJ speed. Figures 9, 10 and 11 provide the instantaneous snapshots for these cases. It is seen that a strong detonation wave does not exist in any of these cases. The variation in temperature not only changes the pre-detonation mixture temperature but also the injection velocities. As a result, it is not guaranteed that the 800 K case, which nominally should be more reactive given only the temperature, shows a weaker detonation structure as compared to the 600 K case. For an increase in mixture temperature, the ideal CJ speed should decrease. However, the computations show that there is an increase in wave speed with mixture temperature. It is important to note that the wave speeds in the RDE are computed by tracking a pressure pulse near the outer wall as a function of time. The wave speed is then the time between two pressure jumps, where a jump is defined as an appreciable increase is pressure beyond the baseline pressure computed in the region downstream of the oxidizer throat. Hence, there is some ambiguity in the wave speed, especially when the pressure pulses are not strong.

However, an interesting aspect of these cases is that the equivalence ratio variations are not as strong as in the ethylene/hydrogen case. In fact for all conditions studied, there is a large region of near stoichiometric composition present in the domain. However, a strong detonation wave is not being supported, with the peak pressure in the domain only 3-4 times atmospheric pressure (compared to von Neumann pressure of 30 atm for ideal wave). However, there is clearly a trailing high temperature zone behind this wave (seen in the red box for temperature in Fig. 10). This is an indication that the azimuthal wave does introduce some heat release and fuel oxidation. However, much of the heat release appears away from this wave, at pressure conditions that are close to atmospheric in a partially-premixed combustion process. From the equivalence ratio contours, it can be see that both rich and lean mixtures are present, but the temperature profiles are relatively agnostic to these variations. This shows that there is continued mixing after the heat release process, which is homogenizing the temperature and post-combustion products.

These cases show that the weak wave is part detonation, and part induced by the fuel-air injection process. For instance, the density variations in the near-injector region creates acoustic perturbations that may be amplified by the heat-release process and turned into an azimuthally propagating wave. However, the slow ignition time scales at these conditions combined with equivalence ratio variations lead to a weak detonation process, where the reaction zones are highly detached from the wave but follow its direction due to the induced flow.

IV. Conclusions and Future Work

Detailed simulations of ethylene-based RDEs were conducted for a range of operating conditions, and one case with hydrogen dilution. The simulations showed that the experimentally observed wave suppression might be related to the existence of multiple combustion modes. In the case with hydrogen dilution, it was observed that the combustor switches between a strong and weak mode, resulting in propagation speeds that are much lower than the ideal wave speeds. It is hypothesized that the two modes arise due to different phenomena: the strong mode is formed when

the mixing and detonation processes reach a synchronized state, while the weak mode is at the other end where the mixing processes are trying to recover after the passage of a detonation wave. While these features are present even in pure hydrogen RDEs, the strong detonation waves observed there dominate the energy conversion process. Due to the relatively weak detonability of ethylene, the time to recovery is much longer. In the pure ethylene-based operation, only the weak mode is observed. As a result, fuel oxidation occurs predominantly in the deflagaration mode, supported by the slow axial velocity in the domain. The transverse injection aids mixing, while the weak azimuthal wave propagation consists of a trailing flow that enables ignition. Overall, the pressure rise in these pure-ethylene systems are not high, ranging from 3-4 times the baseline pressure.

These simulations support the experimental observations, but this does not guarantee that both simulations and experiments produce particular features for the same reasons. While more high-fidelity experiments are necessary for validation, these simulations could be used to determine the characteristics of these weak waves. It is interesting that even though these waves are weak, they sustain over many cycles by inducing a weak reaction zone. These simulations should be explored further to determine the source of these waves, and the impact of the injection process on the combustion process, and subsequent wave propagation speeds..

References

[1] Kailasanath, K., "Recent developments in the research on pulse detonation engines," *AIAA journal*, Vol. 41, No. 2, 2003, pp. 145–159.

[2] Zhou, R., Wu, D., and Wang, J., "Progress of continuously rotating detonation engines," *Chinese Journal of Aeronautics*, Vol. 29, No. 1, 2016, pp. 15–29.

[3] Lisanti, J. C., and Roberts, W. L., "Design of an actively valved and acoustically resonant pulse combustor for pressure-gain combustion applications," *54th AIAA aerospace sciences meeting. San Diego, California*, 2016.

[4] Kailasanath, K., "The rotating-detonation-wave engine concept: a brief status report," *49th AIAA Aerospace Sciences Meeting*, 2011, pp. 2011–0580.

[5] Cocks, P. A., Holley, A. T., and Rankin, B. A., "High fidelity simulations of a non-premixed rotating detonation engine," *54th AIAA Aerospace Sciences Meeting*, 2016, pp. 2016–0125.

[6] Rankin, B. A., Richardson, D. R., Caswell, A. W., Naples, A., Hoke, J. L., and Schauer, F. R., "Imaging of OH* chemiluminescence in an optically accessible nonpremixed rotating detonation engine," *53rd AIAA Aerospace Sciences Meeting*, 2015, pp. 2015–1604.

[7] Irvin Glassman, N. G. G., Richard A. Yetter, *Combustion, Fifth Edition*, Academic Press, 2014.

[8] Bykovskii, F. A., Zhdan, S. A., and Vedernikov, E. F., "Continuous spin detonations," *Journal of Propulsion and Power*, Vol. 22, No. 6, 2006, p. 1204.

[9] Thomas, G., and Williams, R. L., "Detonation interaction with wedges and bends," *Shock waves*, Vol. 11, No. 6, 2002, pp. 481–492.

[10] Stechmann, D. P., Heister, S. D., and Sardeshmukh, S. V., "High-pressure Rotating Detonation Engine Testing and Flameholding Analysis with Hydrogen and Natural Gas," *55th AIAA Aerospace Sciences Meeting, 9 - 13 January 2017, Grapevine, Texas*, 2017, p. 1931.

[11] Schwer, D. A., and Kailasanath, K., "Assessment of Rotating Detonation Engines with Fuel Blends," *53rd AIAA/SAE/ASEE Joint Propulsion Conference*, 2017, p. 4942.

[12] Cho, K. Y., Codoni, J. R., Rankin, B. A., Hoke, J., and Schauer, F., "High-Repetition-Rate Chemiluminescence Imaging of a Rotating Detonation Engine," *54th AIAA aerospace sciences meeting*, 2016, p. 1648.

[13] Wilhite, J., Driscoll, R. B., St. George, A. C., Anand, V., and Gutmark, E. J., "Investigation of a rotating detonation engine using ethylene-air mixtures," *54th AIAA Aerospace Sciences Meeting*, 2016, p. 1650.

[14] Fujii, J., Kumazawa, Y., Matsuo, A., Nakagami, S., Matsuoka, K., and Kasahara, J., "Numerical investigation on detonation velocity in rotating detonation engine chamber," *Proceedings of the Combustion Institute*, Vol. 36, No. 2, 2017, pp. 2665–2672.

[15] Schwer, D., and Kailasanath, K., "Fluid dynamics of rotating detonation engines with hydrogen and hydrocarbon fuels," *Proceedings of the Combustion Institute*, Vol. 34, No. 2, 2013, pp. 1991–1998.

[16] New, T., Panicker, P., Lu, F., and Tsai, H., "Experimental investigations on DDT enhancements by Schelkin spirals in a PDE," *44th AIAA Aerospace Sciences Meeting and Exhibit*, 2006, p. 552.

[17] Varatharajan, B., Petrova, M., Williams, F., and Tangirala, V., "Two-step chemical-kinetic descriptions for hydrocarbon–oxygen-diluent ignition and detonation applications," *Proceedings of the Combustion Institute*, Vol. 30, No. 2, 2005, pp. 1869–1877.

[18] Lu, F., and Braun, E. M., "Rotating Detonation Wave Propulsion: Experimental Challenges, Modeling, and Engine Concepts," *Journal of Propulsion and Power*, Vol. 30, No. 5, 2014, pp. 1125–1142.

[19] Sato, T., Voelkel, S., and Raman, V., "Analysis of detonation structures with hydrocarbon fuels for application towards rotating detonation engines," , 2018. Accepted for AIAA/SAE/ASEE Joint Propulsion Conference in 2018.

[20] Masselot, D., Fiévet, R., and Raman, V., "Effect of Equivalence Ratio and Turbulence Fluctuations on the Propagation of Detonations," *55th AIAA Aerospace Sciences Meeting*, 2017, p. 0374.

[21] Prakash, S., Fiévet, R., Raman, V., Burr, J., and Yu, K. H., "Analysis of the detonation wave structure in a linearized rotating detonation engine," 2018. Submitted to AIAA Journal special issue on Continuous Detonation and its Applications.

[22] Prakash, S., Fievet, R., Raman, V., Burr, J. R., and Yu, K. H., "Numerical Study of the Detonation Wave Structure in a Linear Model Detonation Engine," American Institute of Aeronautics and Astronautics, 2018.

[23] Sato, T., Voelkel, S., and Raman, V., "Detailed Chemical Kinetics based Simulation of Detonation Containing Flows," , 2018. Submitted to ASME Turbo Expo.

[24] Li, C., Kailasanath, K., and Oran, E. S., "Detonation Structures Behind Oblique Shocks," *Physics of Fluids*, Vol. 6, No. 4, 1994, pp. 1600–1611. doi:10.1063/1.868273.

[25] Sato, T., and Raman, V., "Analysis of detonation structures with hydrocarbon fuels for rotating detonation engines applications," , 2018. Submitted to Journal of Propulsion and Power (10/24/2018).

[26] Goodwin, D., Malaya, N., Moffat, H., and Speth, R., "Cantera: An Object Oriented Software Toolkit for Chemical Kinetics, Themodynamics, and Transport Processes, Version 2.1.1," , 2012.

[27] Hassanaly, M., Koo, H., Lietz, C. F., Chong, S. T., and Raman, V., "A minimally-dissipative low-Mach number solver for complex reacting flows in OpenFOAM," *Computer and Fluids*, Vol. 162, 2018, pp. 11–25.

[28] Chong, S. T., Raman, V., Mueller, M. E., and Im, H. G., "The Role of Recirculation Zones in Soot Formation in Aircraft Combustors," *ASME Turbo Expo 2018: Turbomachinery Technical Conference and Exposition*, American Society of Mechanical Engineers, 2018, pp. V04BT04A008–V04BT04A008.

[29] Chong, S. T., Hassanaly, M., Koo, H., Mueller, M. E., Raman, V., and Geigle, K.-P., "Large eddy simulation of pressure and dilution-jet effects on soot formation in a model aircraft swirl combustor," *Combustion and Flame*, Vol. 192, 2018, pp. 452–472.

[30] Chong, S. T., Raman, V., Mueller, M. E., Selvaraj, P., and Im, H. G., "Effect of soot model, moment method, and chemical kinetics on soot formation in a model aircraft combustor," *Proceedings of the Combustion Institute*, 2018.

[31] Tang, Y., Hassanaly, M., Raman, V., Sforzo, B. A., Wei, S., and Seitzman, J. M., "Simulation of Gas Turbine Ignition Using Large Eddy Simulation Approach," *ASME Turbo Expo 2018: Turbomachinery Technical Conference and Exposition*, American Society of Mechanical Engineers, 2018, pp. V04BT04A007–V04BT04A007.

[32] Tang, Y., Hassanaly, M., and Raman, V., "A Comprehensive Modeling Procedure for Estimating Statistical Properties of Forced Ignition," , 2019. *Submitted*.

[33] Damien Masselot, S. V., Takuma Sato, and Raman., V., "Development of Robust Computational Tools for Rotating Detonation Engines," *10th Mediterranean Combustion Symposium*, 2018.

[34] Greenshields, C. J., Weller, H. G., Gasparini, L., and Reese, J. M., "Implementation of semi-discrete, non-staggered central schemes in a colocated, polyhedral, finite volume framework, for high-speed viscous flows," *International journal for numerical methods in fluids*, Vol. 63, No. 1, 2010, pp. 1–21.

[35] Varatharajan, B., and Williams, F., "Ethylene ignition and detonation chemistry, part 2: Ignition histories and reduced mechanisms," *Journal of Propulsion and Power*, Vol. 18, No. 2, 2002, pp. 352–362.

[36] Araki, T., Yoshida, K., Morii, Y., Tsuboi, N., and Hayashi, A. K., "Numerical analyses on ethylene/oxygen detonation with multistep chemical reaction mechanisms: Grid resolution and chemical reaction model," *Combustion Science and Technology*, Vol. 188, No. 3, 2016, pp. 346–369.

[37] Oran, E. S., Weber., J. W., Stefaniw, E. I., Lefebvre, M. H., and Anderson., J. D., "A Numerical Study of a Two-Dimensional H2-O2-Ar Detonation Using a Detailed Chemical Reaction Model," *Combust. Flame*, Vol. 113, No. 1–2, 1998, pp. 147 – 163. doi:http://dx.doi.org/10.1016/S0010-2180(97)00218-6.

[38] Shimizu, H., Tsuboi, N., and Hayashi, A., "Study of detailed chemical reaction model on hydrogen–air detonation," *39th AIAA aerospace sciences meeting and exhibit, Reno, AIAA paper*, Vol. 478, 2001, p. 2001.

[39] Burr, J., and Yu, K., "Detonation Wave Propagation in an Open Channel with Transverse Jets," *53rd AIAA/SAE/ASEE Joint Propulsion Conference*, 2017, p. 4908.

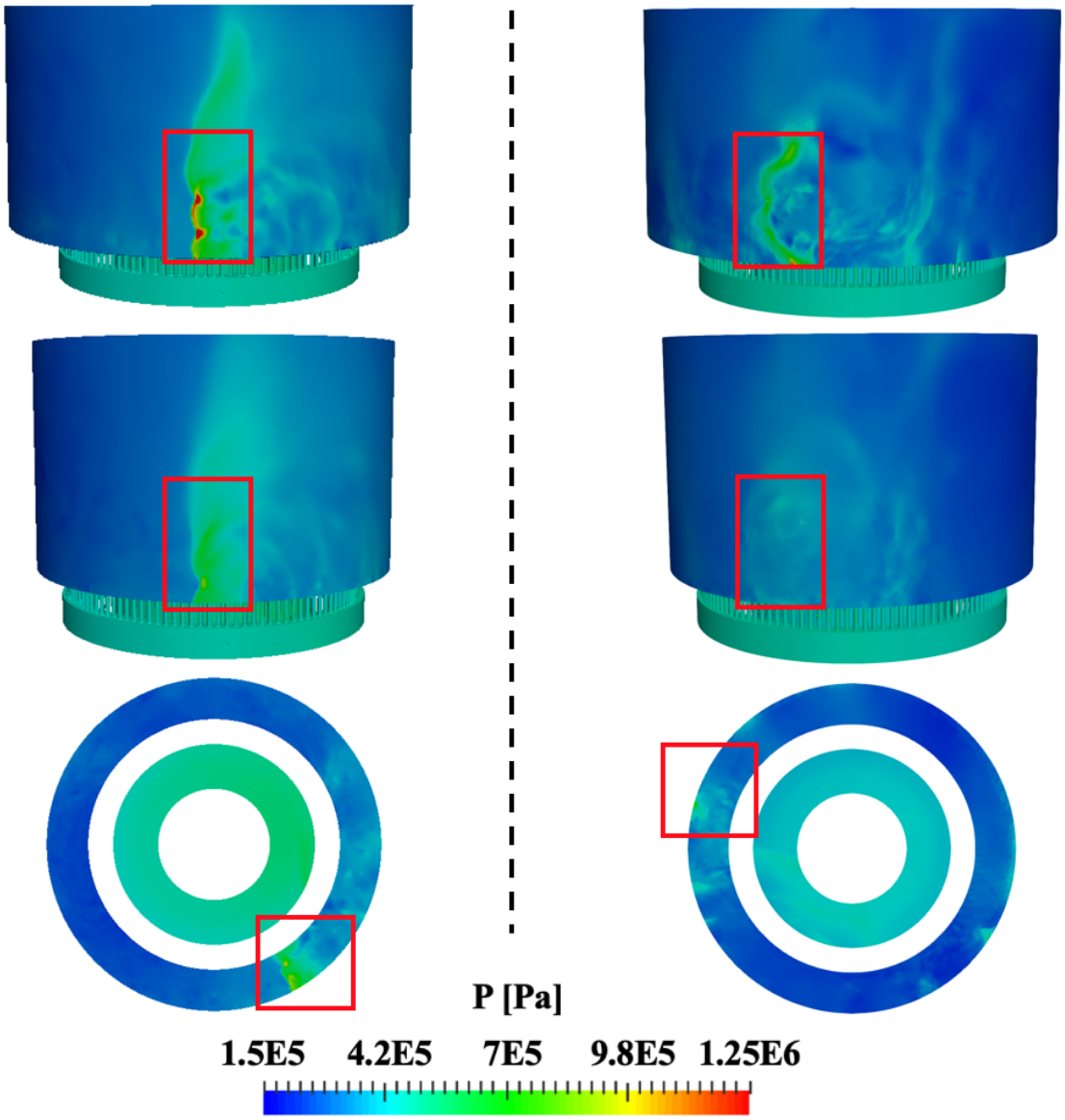

Fig. 6 Pressure field for the C_2H_4:H_2(50:50) mixture case. Top: Near the outer wall. Middle: mid-channel. Bottom: cutting plane 5mm above from the chamber bottom. Left column: strong wave mode. Right column: weak wave mode.

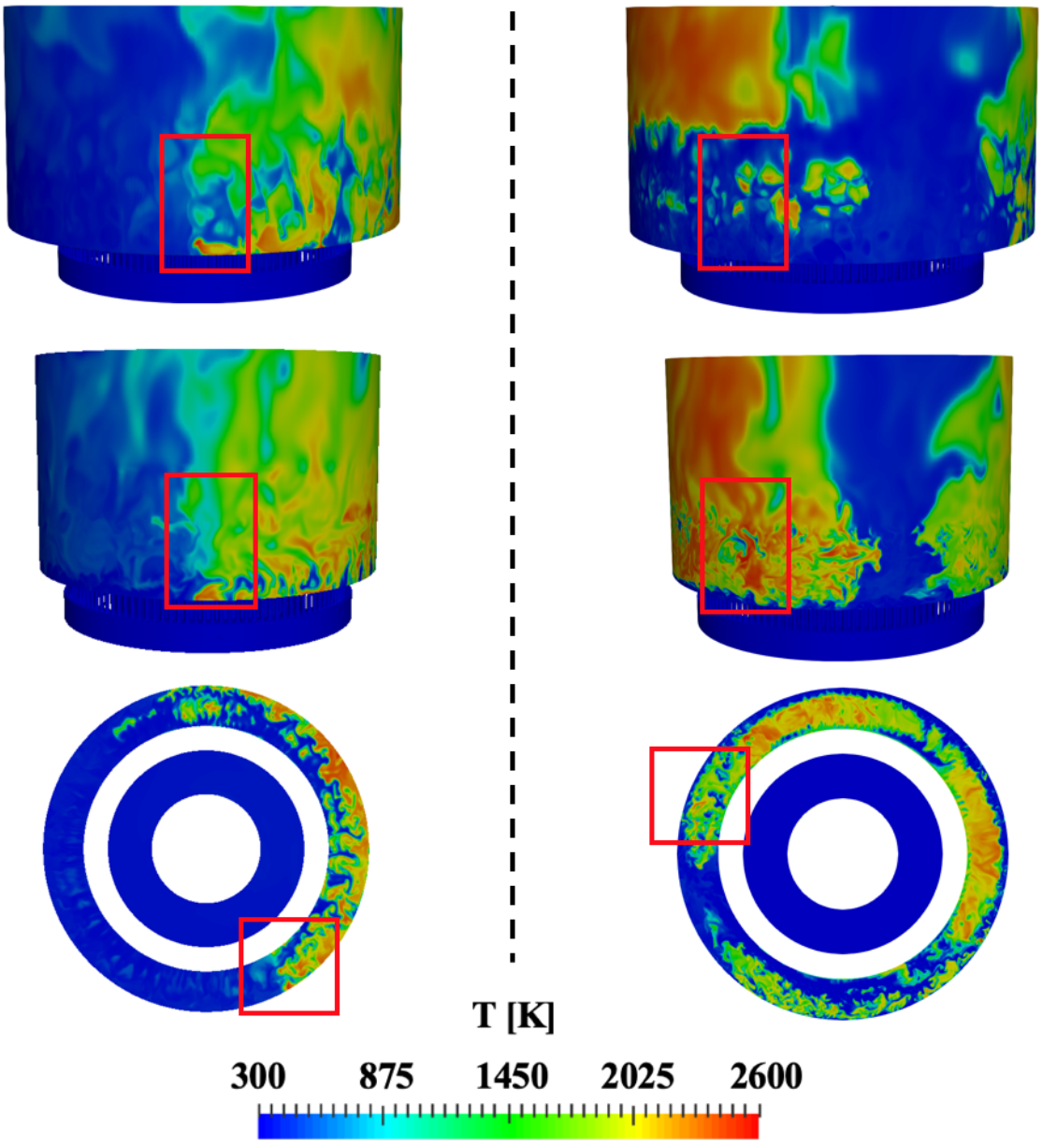

Fig. 7 Temperature field for the C_2H_4:H_2(50:50) mixture case. Top: Near the outer wall. Middle: mid-channel. Bottom: cutting plane 5mm above from the chamber bottom. Left column: strong wave mode. Right column: weak wave mode.

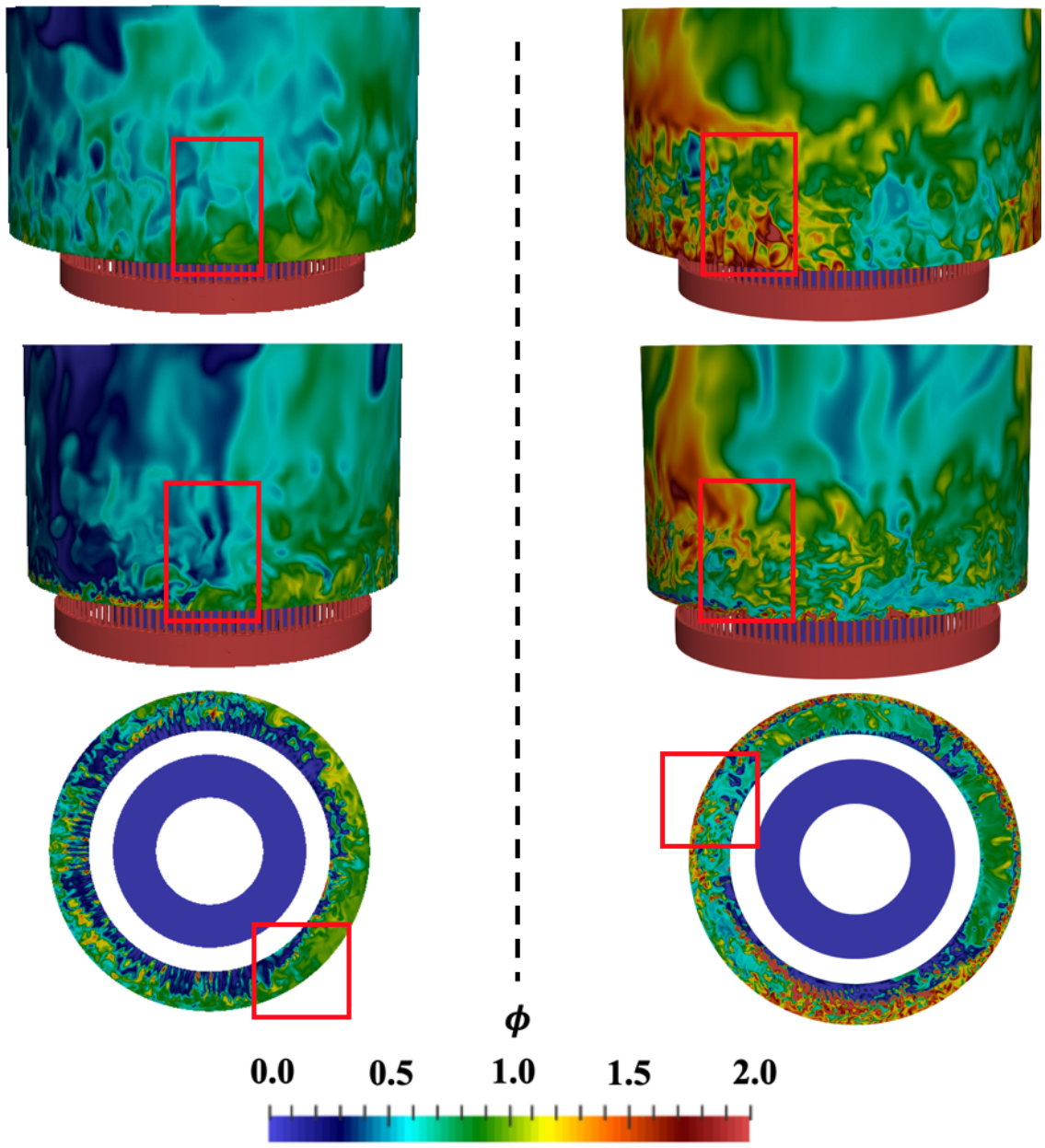

Fig. 8 Equivalence ratio field for the C_2H_4:H_2(50:50) mixture case. Top: Near the outer wall. Middle: mid-channel. Bottom: cutting plane 5mm above from the chamber bottom. Left column: strong wave mode. Right column: weak wave mode.

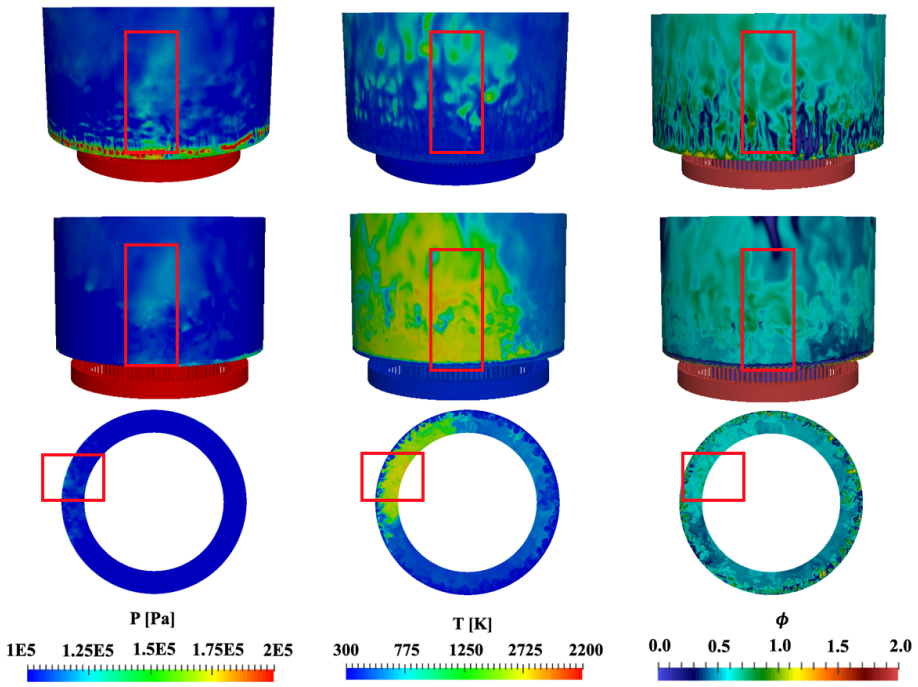

Fig. 9 Pressure, temperature, and equivalence ratio field for the air mass flow T_0 = 400K. Top: Near the outer wall. Middle: mid-channel. Bottom: cutting plane 2cm above from the chamber bottom.

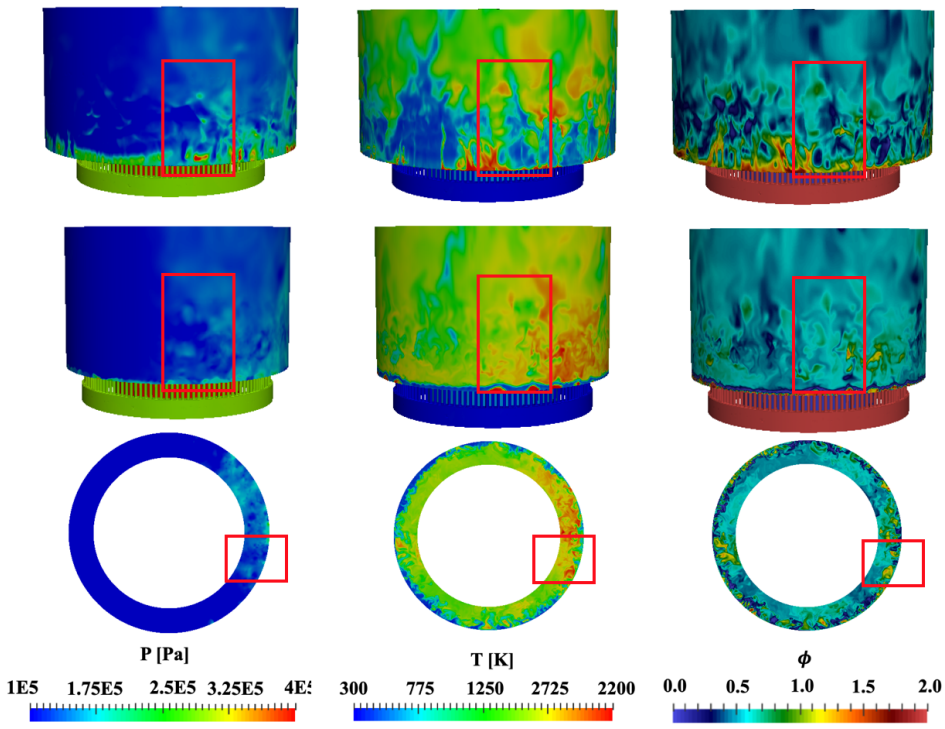

Fig. 10 Pressure, temperature, and equivalence ratio field for the air mass flow T_0 = 600K. Top: Near the outer wall. Middle row: mid-channel. Bottom: cutting plane 2cm above from the chamber bottom.

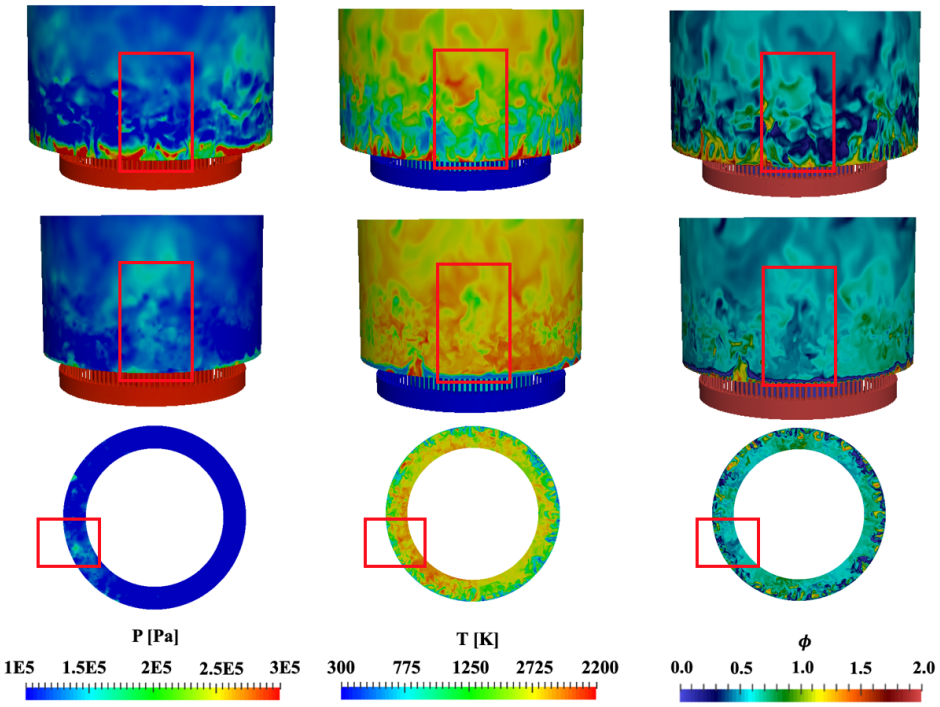

Fig. 11 Pressure, temperature, and equivalence ratio field for the air mass flow T_0 = 800K. Top: Near the outer wall. Middle row: mid-channel. Bottom: cutting plane 2cm above from the chamber bottom.